NIH Public Access
Author Manuscript
J Mol Biol. Author manuscript; available in PMC 2007 October 22.

Published in final edited form as:
J Mol Biol. 2007 May 25; 369(1): 142–156.

Molecular Determinants of Antibiotic Recognition and Resistance by Aminoglycoside Phosphotransferase (3′)-IIIa: A Calorimetric and Mutational Analysis

Malvika Kaul[1], **Christopher M. Barbieri**[1], **Annankoil R. Srinivasan**[1], and **Daniel S. Pilch**[1,2,*]

1 *Department of Pharmacology, University of Medicine and Dentistry of New Jersey-Robert Wood Johnson Medical School, 675 Hoes Lane, Piscataway, NJ 08854-5635*

2 *Department of Chemistry and Chemical Biology, Rutgers University, Piscataway, NJ 08854-8087*

Summary

The growing threat from the emergence of multidrug resistant pathogens highlight a critical need to expand our currently available arsenal of broad-spectrum antibiotics. In this connection, new antibiotics must be developed that exhibit the abilities to circumvent known resistance pathways. An important step toward achieving this goal is to define the key molecular interactions that govern antibiotic resistance. Here, we use site-specific mutagenesis, coupled with calorimetric, NMR, and enzymological techniques, to define the key interactions that govern the binding of the aminoglycoside antibiotics neomycin and kanamycin B to APH(3′)-IIIa (an antibiotic phosphorylating enzyme that produces resistance). Our mutational analyses identify the D261, E262, and C-terminal F264 residues of the enzyme as being critical for recognition of the two drugs as well as the manifestation of the resistance phenotype. In addition, the E160 residue is more important for recognition of kanamycin B than neomycin, with mutation of this residue partially restoring sensitivity to kanamycin B but not to neomycin. By contrast, the D193 residue partially restores sensitivity to neomycin but not to kanamycin B, with the origins of this differential effect being due to the importance of D193 for catalyzing the phosphorylation of neomycin. These collective mutational results, coupled with ^{15}N NMR-derived pK_a and calorimetrically-derived binding-linked drug protonation data, identify the 1-, 3-, and 2′-amino groups of both neomycin and kanamycin B as being critical functionalities for binding to APH(3′)-IIIa. These drug amino functionalities represent potential sites of modification in the design of next-generation compounds that can overcome APH(3′)-IIIa-induced resistance.

Keywords

isothermal titration calorimetry; enzyme binding-linked drug protonation; neomycin; kanamycin B; pyruvate kinase/lactate dehydrogenase-coupled detection of aminoglycoside phosphorylation

Introduction

Aminoglycosides are antibiotics that target the 16 S rRNA A-site and interfere with bacterial protein synthesis.[1,2] The emergence of resistant bacterial strains is endangering the clinical

*Corresponding author: Dr. Daniel S. Pilch, Department of Pharmacology, UMDNJ-Robert Wood Johnson Medical School, 675 Hoes Lane, Piscataway, New Jersey 08854-5635, Tel.: 732-235-3352, Fax: 732-235-4073, E-mail: pilchds@umdnj.edu

Publisher's Disclaimer: This is a PDF file of an unedited manuscript that has been accepted for publication. As a service to our customers we are providing this early version of the manuscript. The manuscript will undergo copyediting, typesetting, and review of the resulting proof before it is published in its final citable form. Please note that during the production process errors may be discovered which could affect the content, and all legal disclaimers that apply to the journal pertain.

NIH-PA Author Manuscript
NIH-PA Author Manuscript
NIH-PA Author Manuscript

NIH-PA Author Manuscript

NIH-PA Author Manuscript

NIH-PA Author Manuscript

utility of aminoglycosides. Although mutations or modifications of the rRNA target sequence, as well as alterations in drug uptake/efflux, are two mechanisms that contribute to aminoglycoside resistance, the most prevalent mechanism of drug resistance encountered clinically involves the expression of drug modifying enzymes.[3] These enzymes covalently modify aminoglycosides through phosphorylation, acetylation, or adenylation, thereby rendering them incapable of binding to their rRNA target. A large number of aminoglycoside-inactivating enzymes that employ one or more of these three modes of drug modification have been identified.[4] These enzymes are subdivided into three main classes, designated as aminoglycoside O-phosphotransferases (APH), N-acetyltransferases (AAC), or O-adenine nucleotidyltransferases (ANT).

The APH enzymes catalyze the transfer of the γ-phosphate of ATP to hydroxyl functionalities of aminoglycosides.[5,6] The largest subfamily of APH enzymes is designated APH(3′), of which APH(3′)-IIIa is a member. APH(3′)-IIIa is very promiscuous in its substrate selection, being able to phosphorylate the 3′- and 5″-hydroxyl functionalities of 4,5-disubstituted 2-deoxystreptamine (2-DOS) aminoglycosides (which include neomycin (Neo) and paromomycin (Par)), as well as the 3′-hydroxyl functionalities of 4,6-disubstituted 2-DOS aminoglycosides (which include kanamycin A (KanA) and kanamycin B (KanB)).[5,6] The catalytic properties of APH(3′)-IIIa have been investigated by Wright and coworkers, who identified the C-terminal domain of the enzyme as being critical for catalysis and resistance.[7–10]

The development of new antibiotics that can overcome APH(3′)-IIIa-induced resistance requires knowledge of the specific interactions that drive drug-enzyme recognition. Toward this end, recent crystallographic studies have yielded structures of ADP-bound APH(3′)-IIIa in complex with Neo or KanA.[11] These structures have provided important insights into the nature of the aminoglycoside binding sites on the enzymes, as well as the amino acid residues that are involved in interactions with the drug substrates. In particular, they have revealed that the drug binding pocket of the enzyme is lined with acidic residues that form electrostatic contacts with numerous drug amino groups. This structural picture is consistent with previous studies by the Mobashery group, which highlighted the importance of drug-enzyme electrostatic contacts for the manifestation of enzyme-mediated resistance.[12]

Inspection of the structural database alone is not sufficient for the identification of the key contacts that stabilize the drug-enzyme complex. Here, we describe a two-pronged approach for deriving the requisite information. (i) We use calorimetric and NMR techniques to identify the specific amino groups of Neo and KanB (see structures in Figure 1) whose protonation is linked to the APH(3′)-IIIa binding reaction. (ii) We systematically mutate eight amino acid residues that form contacts with the amino groups of Neo and KanB, and examine the impact of these mutations on drug-enzyme binding affinity, enzyme catalysis, and APH(3′)-IIIa-mediated resistance. Our collective results highlight the D261, E262, and the C-terminal F264 residues of the enzyme as well as the 1-, 3-, and 2′-amino groups of KanB and Neo as being particularly important functionalities for determining both drug-enzyme recognition and enzyme-mediated resistance.

Results and Discussion

The binding of KanB and Neo to APH(3′)-IIIa is linked to drug protonation

We used isothermal titration calorimetry (ITC) to characterize the binding of KanB and Neo to APH(3′)-IIIa at pH values ranging from 7.5 to 8.5. At each pH value, ITC experiments were conducted in two different buffers (EPPS and TAPS), which differ with respect to their ionizations heats (ΔH_{ion}).13 Figures 2 shows the ITC profiles for the binding of Neo at pH 7.5 (panels (a)–(c)), 8.0 (panels (d)–(f)), and 8.5 (panels (g)–(i)), while Figure 3 shown the

NIH-PA Author Manuscript

NIH-PA Author Manuscript

NIH-PA Author Manuscript

corresponding ITC profiles for the binding of KanB at pH 7.5 (panels (a)–(c)) and 8.0 (panels (d)–(f)). The low binding affinity of KanB for APH(3′)-IIIa (association constant $K_a < 10^4$ M^{-1}) at pH 8.5 precluded our being able to generate ITC profiles at this pH that could be rigorously analyzed. At each pH value, the observed heat of drug binding is more exothermic (negative) in EPPS buffer (ΔH_{ion} = +5.15 kcal/mol) than in TAPS buffer (ΔH_{ion} = +9.92 kcal/mol). The differential binding heats exhibited by the two drugs in EPPS and TAPS buffers is indicative of drug-enzyme binding being coupled to protonation of the drug.[14,15] The number of protons (Δn) linked to binding at a given pH can be determined by simultaneous solution of the following two equations:[16]

$$\Delta H_{obs1} = \Delta H_{corr} + \Delta H_{ion1}\Delta n \quad (1a)$$

$$\Delta H_{obs2} = \Delta H_{corr} + \Delta H_{ion2}\Delta n \quad (1b)$$

In these equations, the numerical subscripts refer to the different buffers, ΔH_{obs} is the observed binding enthalpy in a given buffer, while ΔH_{corr} is the binding enthalpy corrected for buffer ionization effects. A positive value of Δn is indicative of a net uptake of protons, while a negative value of Δn is indicative of a net release of protons.

We determined the requisite ΔH_{obs} values at each pH by analyzing the ITC profiles shown in Figures 2 and 3. Note that a model for a single set of binding sites did not satisfactorily fit any of the drug-APH ITC profiles, an observation that contrasts results previously reported by the Serpersu group.[15] Instead, the ITC profiles were best fit by a model for two independent binding sites. The binding parameters to emerge from these fits are shown in Table 1. Both KanB and Neo bind to APH(3′)-IIIa with an overall stoichiometry of two drug molecules per enzyme. Furthermore, the affinity of the first drug molecule for the enzyme is approximately 28- to 117-fold greater than that of the second drug molecule. This observation suggests that the binding of the first drug molecule reflects a specific interaction with a unique high-affinity site on the enzyme, while the binding of the second drug molecule reflects a secondary nonspecific interaction. We assign the first (high-affinity) binding interaction to the single binding site observed in previously reported crystal structures of APH(3′)-IIIa in complex with either KanA or Neo.[11]

Using the ΔH_1 values listed in Table 1 as the values of ΔH_{obs} in equations (1a) and (1b), we calculated the ΔH_{corr} and Δn values that accompany the specific binding of KanB and Neo to APH(3′)-IIIa at each pH value studied, with the resulting values being listed in Table 2. For each drug, the magnitude of ΔH_{corr} and Δn increases with increasing pH, a pattern reflecting increasing extents of binding-linked drug protonation with increasing pH. This behavior, in turn, causes apparent drug affinity for APH(3′)-IIIa to decrease with increasing pH (see Table 1), since binding-linked protonation reactions are entropically costly.[17]

We sought to confirm our Δn values listed in Table 2, which were calculated using the two-buffer approach described above, by conducting additional ITC characterizations of Neo and KanB binding to APH(3′)-IIIa at pH 7.5 in TES buffer (ΔH_{ion} = +7.83 kcal/mol[13]). In this way, Δn values can be determined from the slopes derived from linear regression analyses of plots of ΔH_{obs} versus ΔH_{ion}, which are shown in Figure S1 of the Supplementary Material. Significantly, the Δn values so determined (1.79 for Neo and 1.66 for KanB) are nearly identical to the corresponding values listed in Table 2 (1.78 for Neo and 1.68 for KanB), thereby validating the two-buffer approach for calculating Δn.

Note that the values of Δn listed in Table 2 reflect contributions from all the drug amino groups whose protonation is linked to APH(3′)-IIIa complex formation. In fact, the number of drug amino groups involved in enzyme binding-linked proton uptake reactions at a given pH can

NIH-PA Author Manuscript

NIH-PA Author Manuscript

NIH-PA Author Manuscript

exceed the magnitude of the observed Δ*n* at that pH. In order to define the relevant number of drug amino groups that participate in enzyme binding-linked protonation reactions, as well as the identities of those groups, one must determine the pK_a value of each drug amino group. The section that follows describes our use of natural abundance ^{15}N NMR to determine the pK_a values of the Neo and KanB amino groups.

Identification of specific drug amino groups whose protonation is linked to APH(3′)-IIIa complex formation: The 1-, 3-, and 2′-amino groups of KanB and the 3-, 2′-, 6′-, 2 ‴-, and 6 ‴-amino groups of Neo

To derive the requisite pK_a values of the amino groups of Neo and KanB, we monitored the pH dependence of the ^{15}N chemical shifts of each drug. The resulting pH profiles are shown in Figure 4. We have previously shown that the free base forms of the drugs must be used in such determinations, since the anions present in the salt forms influence the pH dependencies of the observed ^{15}N chemical shifts at the drug concentrations required for the natural abundance ^{15}N NMR experiments.[17,18] To this end, we used the free base forms of KanB and Neo in our ^{15}N NMR characterizations. We analyzed the pH-dependent ^{15}N NMR data shown in Figure 4 as described in the Materials and Methods to yield the pK_a values listed in Table 3. Note that the pK_a values of the Neo amino groups range from 6.16 (for the 3-amino group) to 9.13 (for the 6‴-amino group), with the corresponding pK_a values of the KanB amino groups ranging from 6.34 (for the 3-amino group) to 8.96 (for the 6′-amino group).

Armed with the pK_a values listed in Table 3, we can calculate (using the standard Henderson-Hasselbalch relationship) the fraction of each drug amino group that exists in the deprotonated NH_2 state at any given pH (f_{NH_2}). Using an approach that we have previously detailed,[14] we identified specific drug amino groups whose protonation is linked to APH(3′)-IIIa complex formation by comparing all possible combinations of f_{NH_2}values for each drug at the differing pH values with the corresponding ITC-derived Δ*n* values. In the case of KanB, such an analysis is consistent with drug binding to the enzyme being linked to protonation of the 3- and 2′-amino groups, as well as either the 1- or the 3″-amino group (but not both). In the case of Neo, the same analysis reveals the protonation of the 3-, 2′-, 6′-, and 2‴-amino groups, but not the 1-amino group, to be linked to APH(3′)-IIIa binding. Note that the 6′-amino group of KanB is not sufficiently deprotonated at pH 8.0 to allow us to rigorously assess whether its protonation is linked to APH(3′)-IIIa binding, with the same being true of the 6‴-amino group of Neo at pH 8.5.

We sought to further refine our assigned identities of the Neo and KanB amino groups whose protonation is linked to APH(3′)-IIIa binding using a computational approach. For this approach, we used the crystal structures of the Neo-APH(3′)-IIIa and KanA-APH(3′)-IIIa complexes reported by Fong and Berghuis as our starting structures.[11] We changed the 2′-hydroxyl group of KanA in the KanA-APH(3′)-IIIa complex to an amino functionality, thereby converting the KanA molecule to KanB. We then calculated the total energies (E_{tot}) associated with both the KanB-APH(3′)-IIIa and Neo-APH(3′)-IIIa complexes in which all the drug amino groups were in their fully-protonated NH_3^+ forms. We further explored the impact on E_{tot} of systematically converting each drug amino group from its protonated NH_3^+ form to its deprotonated NH_2 form. The resulting changes in E_{tot} (ΔE_{tot}) are listed in Table 4. In both drug-enzyme complexes, deprotonation of any of the drug amino groups induces an unfavorable change in E_{tot} (i.e., a positive ΔE_{tot}). In the KanB-APH(3′)-IIIa complex, the magnitude of ΔE_{tot} is significantly greater for deprotonation of the 1-, 3-, and 2′-amino groups (+332, +325, and +271 kcal/mol, respectively) than for deprotonation of the 3″-amino group (+88 kcal/mol). Recall that our buffer-dependent ITC studies were consistent with enzyme binding being linked to protonation of the 3- and 2′-amino groups along with either the 1- or the 3″-amino group (but not both). However, we could not identify whether the 1- or the 3″-

NIH-PA Author Manuscript

NIH-PA Author Manuscript

NIH-PA Author Manuscript

amino group has its protonation linked to enzyme binding since both amino groups exhibit similar pK_a values. Our computational results suggest that enzyme binding is linked to protonation of the 1- and not the 3″-amino group. The ΔE_{tot} value for deprotonation of the KanB 6′-amino group (+169 kcal/mol) lies between those for deprotonation of the 1-, 3-, and 2′-amino groups and that for deprotonation of the 3″-amino group, thereby precluding our being able to resolve the uncertainty as to whether protonation of the KanB 6′-amino group is linked to enzyme binding.

In the Neo-APH(3′)-IIIa complex, the ΔE_{tot} value for deprotonation of the 1-amino group (+299 kcal/mol) is lower than those for deprotonation of the other five amino groups (which range from +316 to +447 kcal/mol). Recall that our buffer-dependent ITC studies were consistent with enzyme binding being linked to protonation of the 3-, 2′-, 6′-, and 2‴-amino groups, but not the 1-amino group. Our computational results are fully consistent with this assignment, while also suggesting that enzyme binding may be linked to protonation of the 6‴-amino group as well.

In the aggregate, our buffer-dependent ITC and computational studies are consistent with the following APH(3′)-IIIa binding-linked drug protonation assignments: For Neo, binding is linked to protonation of the 3-, 2′-, 6′-, and 2‴-amino groups, but not the 1-amino group. For KanB, binding is linked to protonation of the 1-, 3-, and 2′-amino groups, but not the 3″-amino group.

The identities of the drug amino groups whose protonation is linked to enzyme binding in the absence of cofactor are maintained in the presence of cofactor

We sought to determine whether the identities of the drug amino groups whose protonation is linked to APH(3′)-IIIa binding in the absence of cofactor versus are affected by cofactor presence. To this end, we conducted ITC experiments in both EPPS and TAPS buffers to examine the buffer-dependence of ΔH_{obs} for the binding of the ATP cofactor analog adenosine 5′-(β,γ-imido)triphosphate (AMP-PNP) to the KanB-APH(3′)-IIIa and Neo-APH(3′)-IIIa complexes at pH 8.0. The resulting ITC profiles are shown in Figure 5. Note that the ITC profiles for the binding of AMP-PNP to the Neo-APH(3′)-IIIa complex in the two buffers are essentially superimposable (Figure 5(c)), with the same being true for the binding of AMP-PNP to the KanB-APH(3′)-IIIa complex (Figure 5(f)). These results suggest that the binding of AMP-PNP to either drug-APH(3′)-IIIa complex is *not* coupled to any protonation reactions. The binding parameters (listed in Table 5) derived from fits of the ITC profiles in Figure 5 with a model for one set of binding sites provide quantitative support for this conclusion. Significantly, the ΔH_{obs} values for the binding of AMP-PNP to either drug-enzyme complex are similar in EPPS versus TAPS buffer, with any differences being essentially within the experimental uncertainty. These collective results indicate that our assignment of the drug amino groups whose protonation is linked to enzyme binding in the absence of cofactor is preserved in the presence of cofactor. This latter observation contrasts that previously reported by Özen and Serpersu[15], which implied that the extent of binding-linked protonation differed in the binary (drug-enzyme) relative to the ternary (drug-enzyme-cofactor) complex. One potential explanation for the discrepancy between the two results is the absence of magnesium ions in the experiments conducted by Özen and Serpersu. Magnesium ions have been shown to be integral components of the ternary complex.[6,11]

Systematic mutation of amino acids in the drug binding pocket of APH(3′)-IIIa: Impact on structure, resistance, drug binding affinity, and catalysis

We systematically disrupted the drug-enzyme contacts schematically depicted in Figure 1 by site-directed mutagenesis of specific amino acids that interact with one or more of the drug amino groups. Specifically, we created the following eight mutant forms of APH(3′)-IIIa:

NIH-PA Author Manuscript

NIH-PA Author Manuscript

NIH-PA Author Manuscript

E157A, E160A, D190A, D193A, E230A, D261A, E262A, and ΔF264. We then determined the impact of each mutation on enzyme structure, bacterial resistance, the catalytic activity of the enzyme, and the affinity of the enzyme for both KanB and Neo.

Impact on enzyme structure—When introducing specific mutations into a protein, it is important to assess the impact, if any, of the mutations on the structure of the protein. We used circular dichroism (CD) spectroscopy to monitor the impact of each mutation noted above on the structure of APH(3′)-IIIa. The resulting CD spectra are shown in Figure 6. None of the mutations alter the CD spectrum of APH(3′)-IIIa to a significant degree, an observation suggesting that the structure of the enzyme is not appreciably altered by any of the mutations. We further explored the veracity of this conclusion by using the CDNN software suite[19] to deconvolute the CD spectra of APH(3′)-IIIa and its mutant forms into the constituent chiral contributions of individual secondary structural elements (α-helix, antiparallel and parallel β-sheet, β-turn, and random coil). Table S1 lists the mean percentage of each secondary structural element among all eight APH(3′)-IIIa mutants, along with the associated standard deviation. In addition, Table S1 also lists the corresponding percentage of each secondary structural element in the wt enzyme. For each secondary structural element, the percentage in the wt enzyme is similar to the corresponding mean percentage in the mutant enzymes, with the difference being within the standard deviation. These results confirm that none of the mutations significantly perturb the structure of the enzyme. This observation is important, as it indicates that any impacts exerted by the mutations on resistance, drug binding affinity, or enzyme catalysis are not manifestations of mutation-induced perturbations in enzyme structure.

Impact on bacterial resistance—We determined the impact of each mutation on the ability of APH(3′)-IIIa to confer *E. coli* with resistance to KanB and Neo. The bactericidal activities of the two drugs versus *E. coli* BL21 cells that express either no APH(3′)-IIIa, wt APH(3′)-IIIa, or one of the mutant forms of the enzyme are summarized in Table 6. Bacteria that do not express APH(3′)-IIIa are sensitive to both drugs, with the minimal inhibitory concentration (MIC) of each drug being 6 μM. In striking contrast, bacteria that express wt APH(3′)-III are resistant to both drugs, with the MIC value of each drug (1600 μM) being approximately 267-fold higher than that observed versus bacteria that do not express the enzyme. Further inspection of the data in Table 6 reveals that the impact of the mutations on the ability of APH(3′)-IIIa to confer *E. coli* with resistance to KanB and Neo can be classified into the following three categories:

(i) Mutations that essentially abolish the ability of APH(3′)-IIIa to confer resistance The D190A, D261A, E262A and ΔF264 mutations result in MIC values for Neo and KanB that are similar in magnitude to those observed versus bacteria that do not express APH(3′)-IIIa. This observation suggests that the D190, D261, E262 and F264 residues are critical for the resistance phenotype imparted by APH(3′)-IIIa. In subsequent sections, we determine whether the essential nature of these residues is related to their role in drug recognition, enzyme catalysis, or both.

(ii) Mutations that partially compromise the ability of APH(3′)-IIIa to confer resistance The E160A and D193A mutations exhibit differing impacts on the ability of APH (3′)-IIIa to confer resistance to KanB versus Neo. The E160A mutation does not diminish resistance to Neo, with the MIC values for Neo versus bacterial cells that express either wt APH(3′)-IIIa or the E160A mutant form of the enzyme being identical (1600 μM). By contrast, the E160A mutation diminishes (but does not abolish) resistance to KanB, with the MIC value for KanB (400 μM) versus bacteria expressing the E160A mutant APH(3′)-IIIa being four-fold lower than that observed versus bacteria expressing the wt enzyme. Unlike the E160A mutation, the D193A mutation diminishes resistance to Neo, but not to KanB, with the MIC

NIH-PA Author Manuscript

NIH-PA Author Manuscript

NIH-PA Author Manuscript

value for Neo versus bacteria that express the D193A mutant enzyme (200 μM) being eight-fold lower than that observed versus bacteria expressing the wt enzyme. These collective results indicate that E160 plays a role in determining APH(3′)-IIIa-induced resistance to KanB, but not Neo, with the reverse being true of D193.

(iii) Mutations that do not significantly alter the ability of APH(3′)-IIIa to confer resistance The MIC values (800–1600 μM) of Neo and KanB versus bacteria that express either the E157A or E230A mutant form of APH(3′)-IIIa are similar in magnitude to those observed versus bacteria expressing the wt enzyme. Thus, neither E157 nor E230 appears to play a significant role in dictating the resistance phenotype.

Impact on drug binding affinity—We sought to determine how the mutations that compromised (either fully or in part) the ability of APH(3′)-IIIa to confer *E. coli* with the resistance phenotype impact drug recognition. To this end, we used ITC to characterize the impact of each mutation on enzyme affinity for KanB and Neo at pH 7.5. The resulting ITC profiles are shown in Figure 7, with the drug-enzyme association constants (K_a) derived from fits of these profiles being listed in Table 6. Note that the ΔF264, E262A, and D261A mutations are the most deleterious to enzyme affinity for Neo, with these mutations inducing reductions in affinity of 3000-, 2000-, and 323-fold, respectively. The ΔF264, E262A, and D261A mutations are also the most deleterious to enzyme affinity for KanB, reducing K_a by 121-, 7727-, and 2698-fold, respectively. Recall that the F264, E262, and D261 residues are required for APH(3′)-IIIa-induced resistance to Neo and KanB. Our binding affinity data suggest that this requirement is related, at least in part, to the importance of these three residues for drug recognition. Like F264, E262, and D261, the D190 residue is also required for APH(3′)-IIIa-induced resistance to Neo and KanB. However, the D190A mutation decreases enzyme affinity for Neo and KanB by only 22- and 9-fold, respectively. Thus, the requirement of D190 for manifestation of the resistance phenotype does not appear to reflect a correspondingly critical role for this residue in drug recognition.

Further inspection of the data in Table 6 reveals that the E160A mutation reduces enzyme affinity for KanB by 81-fold, while reducing enzyme affinity for Neo by only 30-fold. Thus, E160 plays a more important role in stabilizing the APH(3′)-IIIa complex with KanB than with Neo. It is likely that the differential impact of the E160A mutation on enzyme affinity for KanB versus Neo accounts for our observation that this mutation adversely impacts resistance to KanB but not to Neo. The D193A mutation does not significantly alter enzyme affinity for KanB or Neo. Thus, D193 does not appear to play a significant role in enzyme recognition of either drug. Recall that the D193A mutation partially compromises resistance to Neo but not to KanB. The minimal impact of the D193A mutation on Neo-APH(3′)-IIIa affinity suggests that the partially compromised resistance to Neo associated with this mutation is not the result of a correspondingly compromised ability to bind Neo.

We also determined how the mutations that did not significantly alter the ability of APH(3′)-IIIa to confer *E. coli* with the resistance phenotype (namely E157A and E230A) affected drug-enzyme affinity. These mutations reduced enzyme affinity for KanB and Neo by <6-fold. Such reductions in drug-enzyme affinity do not appear sufficient to compromise resistance.

Impact on catalysis—In addition to using ITC to monitor the impact of the mutations on enzyme affinity for KanB and Neo, we also conducted enzymological assays to determine the corresponding impact of each mutation on the kinetics of APH(3′)-IIIa catalysis. The kinetic parameters to emerge from these studies are listed in Table 6. Inspection of these kinetic parameters reveals the following significant features: (i) The enzyme containing the D190A mutation is catalytically inactive, an observation consistent with previous reports indicating the essential nature of D190 for catalytic activity.[8,10] (ii) The D261A mutation causes a

NIH-PA Author Manuscript

NIH-PA Author Manuscript

NIH-PA Author Manuscript

decrease in turnover number k_{cat} from 1.7 ± 0.1 to 0.02 ± 0.01 s^{-1} ($\Delta k_{cat} = -1.68\ s^{-1}$) when Neo serves as the substrate and from 1.9 ± 0.2 to 0.2 ± 0.01 s^{-1} ($\Delta k_{cat} = -1.7\ s^{-1}$) when KanB serves as the substrate. Thus, the catalytic activity of the D261A mutant enzyme is significantly compromised. In other words, D261 appears to be an important residue for catalysis, as previously suggested by Wright and coworkers.[9] (iii) Deletion of the C-terminal F264 residue also causes a decrease in k_{cat}, although to a lesser extent than that caused by the D261A mutation ($\Delta k_{cat} = -0.8\ s^{-1}$ when Neo serves as the substrate and $-1.0\ s^{-1}$ when KanB serves as the substrate). This result is consistent with F264 playing a role in determining catalytic activity,[9] albeit not as critical a role as played by D261 and D190. (iv) The D193A mutation does not significantly alter the catalytic activity of the enzyme when KanB serves as the substrate. By contrast, this mutation diminishes the catalytic activity of the enzyme when Neo serves as the substrate ($\Delta k_{cat} = -1.0\ s^{-1}$). Thus, D193 appears to be an important residue for catalyzing phosphorylation of Neo but not KanB. (v) Mutation of E157, E160, E230, or E262 does not exert a significant impact on k_{cat}, suggesting that none of these residues play a role in enzyme catalysis

A comparison of the Michaelis (K_m) and K_a constants in Table 6 reveals that the K_m values associated with E262A and ΔF264 mutants are significantly lower than the corresponding values of K_d (i.e., $1/K_a$). This result suggests that the catalytic activities of these two mutant enzymes may not strictly adhere to Michaelis-Menten kinetic principles, which postulate that K_m should be $\geq K_d$. The apparent deviation of the catalytic activities of E262A and ΔF264 from Michaelis-Menten behavior may reflect product inhibition. In such a case, our K_m values for these mutants (as well as those previously reported[9]) would represent underestimates.

Defining the key drug-enzyme interactions that drive APH(3′)-IIIa-induced resistance

The linked protonation, antibacterial, binding affinity, and enzymological results described in the preceding sections provide key insights into the specific drug-enzyme interactions that are important for APH(3′)-IIIa-induced resistance. The most amino acid residues that drive APH (3′)-IIIa binding to both Neo and KanB are D261, E262, and the C-terminal F264 residue. The crystallographic database[11] indicates that these enzymes residues form electrostatic contacts with the 1-, 3-, and 6′-amino groups of both drugs (see Figure 1). The profound energetic contributions that these interactions make to drug-enzyme complex formation are highlighted by our observation that protonation of two of the three drug amino groups involved (the 3- and 6′-amino groups of Neo and the 1- and 3-amino groups of KanB) is coupled to the binding reaction. The critical role that D261, E262, and F264 play in driving drug-enzyme binding underlies the essential nature of these three amino acids for APH(3′)-IIIa-induced resistance. Note that the importance of D261 for resistance also reflects contributions from the role this residue plays in promoting enzyme catalysis, with the same being true of the C-terminal F264 residue (albeit to a lesser extent).

E160 interacts with the 1-amino group of both Neo and KanB (Figure 1), with the energetic contribution of this interaction to drug-enzyme binding being greater for KanB than for Neo. This differential contribution is manifested in the drug-enzyme binding reaction being coupled to protonation of the 1-amino group only when KanB (and not Neo) serves as the enzyme substrate. Recall that the E160A mutation diminished resistance to KanB, but not to Neo. This result is consistent with the greater importance of E160 for driving APH(3′)-IIIa binding to KanB relative to Neo.

D190 has been previously identified as a critical residue for enzyme catalysis and resistance.[8,10] Our results confirm this observation, while also indicating that D190 plays a role in driving formation of the drug-enzyme complex. D190 contributes to the stability of the APH(3′)-IIIa complex with KanB and Neo by virtue of its interaction with the 2′-amino group of each drug,

NIH-PA Author Manuscript

NIH-PA Author Manuscript

NIH-PA Author Manuscript

an interaction that accounts for protonation of this amino group being linked to the APH(3′)-IIIa binding of both drugs.

D193 plays a role in determining resistance to Neo, but not to KanB. Its importance for resistance to Neo is derived from its role in catalyzing the phosphorylation of the drug, rather than from its minimal contributions to drug-enzyme binding affinity. The structural database reveals that D193 does not form contacts with any KanB functionalities, but interacts with the 2‴-amino group of Neo (Figure 1). The energetic contributions from this interaction do not appear to be sufficient in magnitude to drive the observed binding-linked protonation of the 2‴-amino group. In addition to D193, E24 and D231 also interact with the 2‴-amino group (Figure 1). It is likely that one or both of these interactions help drive the binding-linked protonation of the 2‴-amino group.

E157 and E230 do not play important roles in determining drug binding affinity, catalytic activity, or resistance. E230 interacts with the 3″-amino group of KanB and the 6‴-amino group of Neo. However, the strength of these interactions would seem insufficient to drive binding-linked protonation of the 3″- and 6‴-amino groups. Consistent with this notion, our studies indicate that protonation of the 3″-amino group is not linked to the KanB-APH(3′)-IIIa interaction. That said our studies also suggest that the binding of Neo to APH(3′)-IIIa is linked to protonation of the 6‴-amino group of the drug. Besides interacting with E230, this amino group also interacts with D231 (Figure 1), which may facilitate the coupling of its protonation to the enzyme binding reaction. E157 interacts with the 3-amino group of both Neo and KanB. Although protonation of the 3-amino group of each drug is linked to APH(3′)-IIIa binding, this linkage is probably driven to a major extent by the interactions of the 3-amino group with the F264 and D261 residues of the enzyme.

In the aggregate, our results suggest that the 1-, 3-, and 2′-amino groups of both 4,5- and 4,6-disubstituted 2-DOS aminoglycosides are important functionalities for APH(3′)-IIIa recognition. These collective drug functionalities represent sites that upon modification either singly or in combination, have the potential for overcoming APH(3′)-IIIa-induced resistance. The potential of this approach is exemplified by the 4,6-disubstituted 2-DOS aminoglycoside amikacin, which overcomes APH(3′)-IIIa-induced resistance through combined modifications of both the 1- and 2′-amino groups relative to KanB.[7] Clearly, an important consideration in the design of any next-generation compound is to preserve as closely as possible the integrity of the drug interaction with its therapeutic target (the 16 S rRNA A-site).

Materials and Methods

Drugs

Neomycin·3H_2SO_4 was obtained from Sigma, while Kanamycin B·H_2SO_4 was obtained from Fluka. These sulfate salt forms of the drugs were used without further purification in all experiments, with the exception of those using ^{15}N NMR. The NMR studies were conducted using the free base forms of both drugs, which were prepared as previously described.[18] Adenosine 5′-(β,γ-imido)triphosphate (AMP-PNP) and isopropyl β-D-1-thiogalactopyranoside (IPTG) were obtained from Sigma.

Protein Purification

The APH(3′)-IIIa gene was amplified by polymerase chain reaction (PCR) from the pAT21-1 plasmid,[20] which was obtained from Dr. P. Courvalin at the National Reference Center, Institut Pasteur, France. The primers used for PCR were designed such that a unique *Nde*I site and a histidine tag were introduced at the 5′-end of the APH(3′)-IIIa gene, and a unique *Hind*III site was introduced at the 3′-end of the gene. The amplified gene product was digested with *Nde*I

NIH-PA Author Manuscript

NIH-PA Author Manuscript

NIH-PA Author Manuscript

and *Hind*III, and ligated into the pET-22b(+) cloning vector (Novagen), which had been previously digested with the same enzymes. The sequence of the final recombinant plasmid (pETAPH) was verified by sequence analysis, and was used to transform *E. coli* BL21 (DE3) cells. APH(3′)-IIIa protein was isolated from these pETAPH-transformed bacteria by batch/gravity flow affinity purification as described below.

Luria-Bertani media was inoculated with overnight cultures of pETAPH-transformed *E. coli* cells. These freshly inoculated cultures were grown at 37 °C for 6–8 hours (to an absorbance reading of 0.6 at 600 nm), at which point APH(3′)-IIIa production was induced by addition of IPTG to a final concentration of 1 mM. Following addition of IPTG, the cultures were incubated for an additional 2 hours at 37 °C. The cells were then harvested by centrifugation at 12,000g for 20 minutes at 4 °C and lysed using BugBuster™ HT Lysis Buffer (Novagen). The cell lysates were clarified by centrifugation at 16,000g for 30 minutes at 4 °C to remove cell debris. The clarified lysates were then equilibrated with BD TALON™ Metal Affinity Resin (Clontech) for 30–60 minutes at 4 °C to allow the histidine-tagged APH(3′)-IIIa to bind to the resin. The resin was then washed three times with a 10-fold volumetric excess of wash buffer (50 mM sodium phosphate (pH 7.0) and 300 mM NaCl), and subsequently transferred into a gravity-flow column. The resin in the column was then washed once with wash buffer and once with wash buffer containing 10 mM imidazole. APH(3′)-IIIa was eluted from the column with elution buffer (50 mM sodium phosphate (pH 7.0), 300 mM NaCl, and 300 mM imidazole), and 1 mL fractions were collected. The fractions were analyzed by SDS-PAGE to identify those that contained the bulk of the protein. These fractions were pooled and dialyzed into storage buffer containing 10 mM EPPS or TAPS (pH 7.5), 100 mM KCl, 5mM $MgCl_2$, 0.1 mM DTT, and 20% glycerol. The dialyzed protein stock solutions were aliquoted and stored at −20 °C for up to 4 months.

The extinction coefficient at 280 nm and 25 °C ($\varepsilon_{280\text{-}25°C}$) for APH(3′)-IIIa was determined to be 56,460 $M^{-1}\cdot cm^{-1}$ by comparing the absorbance of the protein at 280 nm with the protein concentration as determined using a BCA™ protein assay kit (Pierce). This assay was conducted as per the manufacturer's protocol using bovine serum albumin as a standard. All protein concentrations were determined spectrophotometrically using the value of $\varepsilon_{280\text{-}25°C}$ noted above.

All mutant forms of the enzyme were cloned from the plasmid pETAPH using PCR to introduce the desired point mutations. The sequences of all the mutants were verified by sequencing analyses, and the mutant enzymes were purified in a manner similar to that described above for the wt enzyme.

Isothermal titration calorimetry (ITC)

ITC measurements were performed at 25 °C on a MicroCal VP-ITC. For all ITC experiments, the solution conditions were 10 mM buffer (EPPS, TES, or TAPS) at the desired pH (7.5, 8.0, or 8.5), 100 mM KCl, 5 mM $MgCl_2$, and 0.01% TWEEN 80. In a typical experiment, 5 or 10 μL aliquots of drug were sequentially injected from a 250 μL rotating syringe (300 RPM) into an isothermal sample chamber containing 1.42 mL of a protein solution. Protein concentrations were chosen such that the *c* value (the unitless product of association constant (K_a) × [total protein] × binding stoichiometry (*N*)) fell in the range of 8 to 250. This criterion was fulfilled in all ITC experiments except those with the E262A and ΔF264 mutant forms of APH(3′)-IIIa. The *c* value for the ITC experiments with these two mutants fell below 8, since the affinities of the drugs for these mutant enzymes were very low (with K_a values ranging from 0.42×10^4 to 2.1×10^4). In all the ITC experiments, protein concentrations ranged from 7 to 450 μM, while drug concentrations ranged from 120 μM to 8.0 mM. In each experiment, the initial delay prior to the first injection was 60 seconds. The duration of each 5 and 10 μL injection was 5 and 10 seconds, respectively. The delay between injections ranged from 360 to 600

NIH-PA Author Manuscript

NIH-PA Author Manuscript

NIH-PA Author Manuscript

seconds. Each drug-protein experiment was accompanied by the corresponding control experiment in which equivalent aliquots of the drug were injected into a solution of buffer alone. Each injection generated a heat burst curve (μcal/sec vs. sec). The area under each curve was determined by integration [using the Origin version 5.0 software (MicroCal, Inc.)] to obtain a measure of the heat associated with that injection. The heat associated with each drug-buffer injection was subtracted from the corresponding heat associated with each drug-enzyme injection to yield the heat of drug binding for that injection. The resulting corrected injection heats were best fit by a model for two independent sets of binding sites.

In the AMP-PNP binding experiments, 10 μL aliquots of AMP-PNP at concentrations ranging from 1.7 to 1.8 mM were sequentially injected into a solution containing either Neo-APH(3′)-IIIa or KanB-APH(3′)-IIIa complex at concentrations ranging from 160 to 170 μM. The [drug]/[APH(3′)-IIIa] ratio in all solutions of drug-APH(3′)-IIIa complex was 1.1, a value ensuring that all the enzyme in solution was drug bound. The concentrations of drug-APH(3′)-IIIa complex indicated above resulted in *c* values that fell in the range of 8 to 17. The AMP-PNP experiments noted above were accompanied by corresponding control experiments in which 10 μL aliquots of AMP-PNP were injected into buffer alone. The duration of each injection was 10 seconds and the initial delay prior to the first injection was 60 seconds. The delay between injections was 300 seconds. The heat associated with each AMP-PNP-buffer injection was subtracted from the corresponding heat associated with each injection of AMP-PNP into drug-APH(3′)-IIIa complex to yield the heat of AMP-PNP binding for that injection. The resulting corrected injection heats were best fit by a model for one set of binding sites. The solution conditions for the AMP-PNP ITC experiments contained 10 mM buffer (EPPS or TAPS) at pH 8.0, 100 mM KCl, 5 mM $MgCl_2$, and 0.01% TWEEN 80.

^{15}N NMR Spectroscopy

^{15}N NMR spectra were acquired at 30.4 MHz and 25 °C on a Varian Unity 300 spectrometer using a recycle delay of one second. All ^{15}N chemical shifts are reported relative to NH_3 using 1 M [^{15}N]urea in DMSO (Isotec) as an external reference, with the ^{15}N chemical shift of the reference set to 77.0 ppm. The experimental NMR solutions were prepared by dissolving the 600 mg of Neo free base or 350 mg of KanB free base in 600 μL of 85% H_2O/15% D_2O to yield final drug concentrations of 1.63 and 1.21 M, respectively. The pH of the NMR samples was adjusted by addition of either HCl or KOH in 85% H_2O/15% D_2O. All pH measurements of NMR samples were acquired using a Corning 430 pH meter interfaced with a micro stem glass/calomel combination electrode (Mettler Toledo, Inc.). The assignments of the ^{15}N resonances were based on those previously reported [21–23]. Amino pK_a values were determined from plots of the pH dependence of ^{15}N chemical shifts (δ) by nonlinear least squared analyses using the following relationship:

$$\delta = \frac{\left(\delta_{NH_2} - \delta_{NH_3^+}\right)\left(10^{pH-pK_a}\right)}{1 + \left(10^{pH-pK_a}\right)} + \delta_{NH_3^+} \quad (2)$$

In this relationship, $\delta_{NH_3^+}$ and δ_{NH_2} are the ^{15}N chemical shifts of the amino nitrogens in their protonated and deprotonated states, respectively.

Computational Studies

The crystal structures of the Neo-APH(3′)-IIIa and KanA-APH(3′)-IIIa complexes reported by Fong and Berghuis[11] were used as starting structures (PDB codes 1L8U and 1L8T, respectively). The 2′-hydroxyl group of KanA in the KanA-APH(3′)-IIIa complex was then

NIH-PA Author Manuscript

NIH-PA Author Manuscript

NIH-PA Author Manuscript

changed to an amino functionality using the Molecular Operating Environment (MOE) software package (Chemical Computing Group, Inc.), thereby converting the KanA molecule to KanB. For the initial calculations, all the drug amino groups in both the Neo-APH(3′)-IIIa and KanB-APH(3′)-IIIa complexes were set in their NH_3^+ states using MOE. The partial atomic charges of the fully protonated drug molecules were computed using the antichamber module of the AMBER 8.0 molecular dynamics software package.[24] The drug-APH(3′)-IIIa complexes were then subjected to energy minimization using the AMBER02 force field.[25, 26] Energy minimization was carried out for 1000 steps of steepest-descent, followed by another 1000 steps of conjugate-gradient method. Following these initial calculations, each drug amino group was systematically converted from its protonated NH_3^+ form to its deprotonated NH_2 form, with the complex resulting from each amino group alteration being subjected to the same energy minimization calculations described above. All the calculations were performed on a DELL Xeon Precision 530 workstation.

Circular Dichroism (CD) Spectroscopy

CD experiments were conducted at 25 °C on an AVIV Model 202 spectropolarimeter equipped with a thermoelectrically controlled cell holder. A quartz cell with a 1 mm pathlength was used for all the CD studies. CD spectra were recorded from 260 to 205 nm in 0.5 nm increments with an averaging time of 5 sec. The buffer conditions were 10 mM EPPS (pH 7.5), 100 mM KCl, and 5 mM $MgCl_2$. The enzyme concentration was 10 μM. Buffer-corrected CD spectra were deconvoluted using the CDNN Program[19] trained with a 33 spectra data set.

Antibacterial Assay

The antibacterial activities of Neo and KanB versus wt or mutant APH(3′)-IIIa expressing *E. coli* BL21 (DE3) cells, as well as versus *E. coli* BL21 (DE3) cells expressing no form of APH (3′)-IIIa, were determined using a standard minimum inhibitory concentration (MIC) assay. Log phase bacteria were grown at 37 °C in Luria-Bertani (LB) medium containing two-fold serial dilutions of the drugs to yield final concentrations ranging from 6400 μM to 10 nM. Bacterial growth was monitored after 24 hours by measuring optical density at 620 nm, with the MIC being defined as the lowest drug concentration at which growth is completely inhibited.

Enzyme Assay

Kinetic parameters (k_{cat} and K_m) for wt and mutant APH(3′)-IIIa were determined at 30 °C using a coupled pyruvate kinase/lactate dehydrogenase (PK/LDH) reaction.[7,27] In this assay, the ADP formed upon phosphorylation of Neo and KanB by APH(3′)-IIIa is used as a substrate by PK to form ATP in the presence of phosphoenol pyruvate (PEP). The concomitant oxidation of NADH to NAD by LDH causes a decrease in absorbance at 340 nm, which was monitored in a 4 mm pathlength quartz cuvette using an AVIV 14DS spectrophotometer equipped with a thermoelectrically controlled cell holder. The buffer conditions were 50 mM Tris (pH 7.5), 40 mM KCl, and 10 mM $MgCl_2$. Drug concentrations ranged from 3 to 400 μM, while the ATP and NADH concentrations were kept constant at 1 and 7 mM, respectively. In each enzyme assay, enzyme concentrations ([E]) ranged from 0.9 to 1.1 μM. Initial rates (v) were plotted against drug concentration ([S]) and fit with the following formalism:

$$v = \frac{k_{cat}[E][S]}{K_m + [S]} \quad (3)$$

Supplementary Material

Refer to Web version on PubMed Central for supplementary material.

NIH-PA Author Manuscript

NIH-PA Author Manuscript

NIH-PA Author Manuscript

Acknowledgements

This work was supported by NIH grant CA097123. M.K. was supported by an NIH postdoctoral fellowship (F32 AI62041). C.M.B. was supported by an NIH training grant (5T32 GM08319) in molecular biophysics.

References

1. Moazed D, Noller HF. Interaction of Antibiotics with Functional Sites in 16 S Ribosomal RNA. Nature 1987;327:389–394. [PubMed: 2953976]
2. Puglisi, JD.; Blanchard, SC.; Dahlquist, KD.; Eason, RG.; Fourmy, D.; Lynch, SR.; Recht, MI.; Yoshizawa, S. Aminoglycoside Antibiotics and Decoding. In: Garrett, RA.; Douthwaite, SR.; Liljas, A.; Matheson, AT.; Moore, PB.; Noller, HF., editors. The Ribosome: Structure, Function, Antibiotics, and Cellular Interactions. ASM Press; Washington, D. C: 2000. p. 419-429.
3. Magnet S, Blanchard JS. Molecular Insights into Aminoglycoside Action and Resistance. Chem Rev 2005;105:477–498. [PubMed: 15700953]
4. Shaw KJ, Rather PN, Hare RS, Miller GH. Molecular Genetics of Aminoglycoside Resistance Genes and Familial Relationships of the Aminoglycoside-Modifying Enzymes. Microbiol Mol Biol Rev 1993;57:138–163.
5. Wright GD, Thompson PR. Aminoglycoside Phosphotransferases: Proteins, Structure, and Mechanism. Front Biosci 1999;4:D9–D21. [PubMed: 9872733]
6. Kim C, Mobashery S. Phosphoryl Transfer by Aminoglycoside 3′-Phosphotransferases and Manifestation of Antibiotic Resistance. Bioorg Chem 2005;33:149–158. [PubMed: 15888308]
7. McKay GA, Thompson PR, Wright GD. Broad Spectrum Aminoglycoside Phosphotransferase Type III from *Enterococcus*: Overexpression, Purification, and Substrate Specificity. Biochemistry 1994;33:6936–6944. [PubMed: 8204627]
8. Hon WC, McKay GA, Thompson PR, Sweet RM, Yang DS, Wright GD, Berghuis AM. Structure of an Enzyme Required for Aminoglycoside Antibiotic Resistance Reveals Homology to Eukaryotic Protein Kinases. Cell 1997;89:887–895. [PubMed: 9200607]
9. Thompson PR, Schwartzenhauer J, Hughes DW, Berghuis AM, Wright GD. The COOH Terminus of Aminoglycoside Phosphotransferase (3′)-IIIa Is Critical for Antibiotic Recognition and Resistance. J Biol Chem 1999;274:30697–30706. [PubMed: 10521458]
10. Boehr DD, Thompson PR, Wright GD. Molecular Mechanism of Aminoglycoside Antibiotic Kinase APH(3′)-IIIa: Roles of Conserved Active Site Residues. J Biol Chem 2001;276:23929–23936. [PubMed: 11279088]
11. Fong DH, Berghuis AM. Substrate Promiscuity of an Aminoglycoside Antibiotic Resistance Enzyme via Target Mimicry. The EMBO Journal 2002;21:2323–2331. [PubMed: 12006485]
12. Roestamadji J, Grapsas I, Mobashery S. Loss of Individual Electrostatic Interactions Between Aminoglycoside Antibiotics and Resistance Enzymes As an Effective Means to Overcoming Bacterial Drug Resistance. J Am Chem Soc 1995;117:11060–11069.
13. Fukada H, Takahashi K. Enthalpy and Heat Capacity Changes for the Proton Dissociation of Various Buffer Components in 0.1 M Potassium Chloride. Proteins Struct Funct Genet 1998;33:159–166. [PubMed: 9779785]
14. Kaul M, Barbieri CM, Kerrigan JE, Pilch DS. Coupling of Drug Protonation to the Specific Binding of Aminoglycosides to the A site of 16 S rRNA: Elucidation of the Number of Drug Amino Groups Involved and their Identities. J Mol Biol 2003;326:1373–1387. [PubMed: 12595251]
15. Özen C, Serpersu EH. Thermodynamics of Aminoglycoside Binding to Aminoglycoside-3′-Phosphotransferase IIIa Studied by Isothermal Titration Calorimetry. Biochemistry 2004;43:14667–14675. [PubMed: 15544337]
16. Doyle ML, Louie G, Dal Monte PR, Sokoloski TD. Tight Binding Affinities Determined from Thermodynamic Linkage to Protons by Titration Calorimetry. Methods Enzymol 1995;259:183–194. [PubMed: 8538453]
17. Pilch DS, Kaul M, Barbieri CM. Ribosomal RNA Recognition by Aminoglycoside Antibiotics. Top Curr Chem 2005;253:179–204.

NIH-PA Author Manuscript

NIH-PA Author Manuscript

NIH-PA Author Manuscript

18. Barbieri CM, Pilch DS. Complete Thermodynamic Characterization of the Multiple Protonation Equilibria of the Aminoglycoside Antibiotic Paromomycin: A Calorimetric and Natural Abundance ^{15}N NMR Study. Biophys J 2006;90:1338–1349. [PubMed: 16326918]

19. Böhm G, Muhr R, Jaenicke R. Quantitative Analysis of Protein Far UV Circular Dichroism Spectra by Neural Networks. Protein Eng Des Selec 1992;5:191–195.

20. Trieu-Cuot P, Courvalin P. Nucleotide Sequence of the *Streptococcus faecalis* Plasmid Gene Encoding the 3′5″-Aminoglycoside Phosphotransferase Type III. Gene 1983;23:331–341. [PubMed: 6313476]

21. Botto RE, Coxon B. Nitrogen-15 Nuclear Magnetic Resonance Spectroscopy of Neomycin B and Related Aminoglycosides. J Am Chem Soc 1983;105:1021–1028.

22. Dorman DE, Paschal JW, Merkel KE. ^{15}N Nuclear Magnetic Resonance Spectroscopy. The Nebramycin Aminoglycosides. J Am Chem Soc 1976;98:6885–6888. [PubMed: 965656]

23. Koch KF, Merkel KE, O'Connor SC, Occolowitz JL, Paschal JW, Dorman DE. Structures of Some of the Minor Aminoglycoside Factors of the Nebramycin Fermentation. J Org Chem 1978;43:1430–1434.

24. Case, DA.; Darden, TA.; Cheatham, TE., III; Simmerling, CL.; Wang, J.; Duke, RE.; Luo, R.; Merz, KM.; Wang, B.; Pearlman, DA.; Crowley, M.; Brozell, S.; Tsui, V.; Gohlke, H.; Mongan, J.; Hornak, V.; Cui, G.; Beroza, P.; Schafmeister, C.; Caldwell, JW.; Ross, WS.; Kollman, PA. AMBER 8.0. University of California; San Francisco, San Francisco: 2004.

25. Cornell WD, Cieplak P, Bayly CI, Gould IR, Merz KM Jr, Ferguson DM, Spellmeyer DC, Fox T, Caldwell JW, Kollman PA. A Second Generation Force Field for the Simulation of Proteins, Nucleic Acids, and Organic Molecules. J Am Chem Soc 1995;117:5179–5197.

26. Wang J, Cieplak P, Kollman PA. How Well Does a Restrained Electrostatic Potential (RESP) Model Perform in Calculating Conformational Energies of Organic and Biological Molecules? J Comput Chem 2000;21:1049–1074.

27. Goldman PR, Northrop DB. Purification and Spectrophotometric Assay of Neomycin Phosphotransferase II1. Biochem Biophys Res Commun 1976;69:230–236. [PubMed: 177018]

Abbreviations used

APH
aminoglycoside phosphotransferase

Neo
neomycin

KanB
kanamycin B

KanA
kanamycin A

ITC
isothermal titration calorimetry

2-DOS
2-deoxystreptamine

AMP-PNP
adenosine 5′-(β,γ-imido)triphosphate

IPTG
isopropyl β-D-1-thiogalactopyranoside

PK
pyruvate kinase

NIH-PA Author Manuscript

NIH-PA Author Manuscript

NIH-PA Author Manuscript

LDH

lactate dehydrogenase

PEP

phosphoenol pyruvate

NIH-PA Author Manuscript

NIH-PA Author Manuscript

NIH-PA Author Manuscript

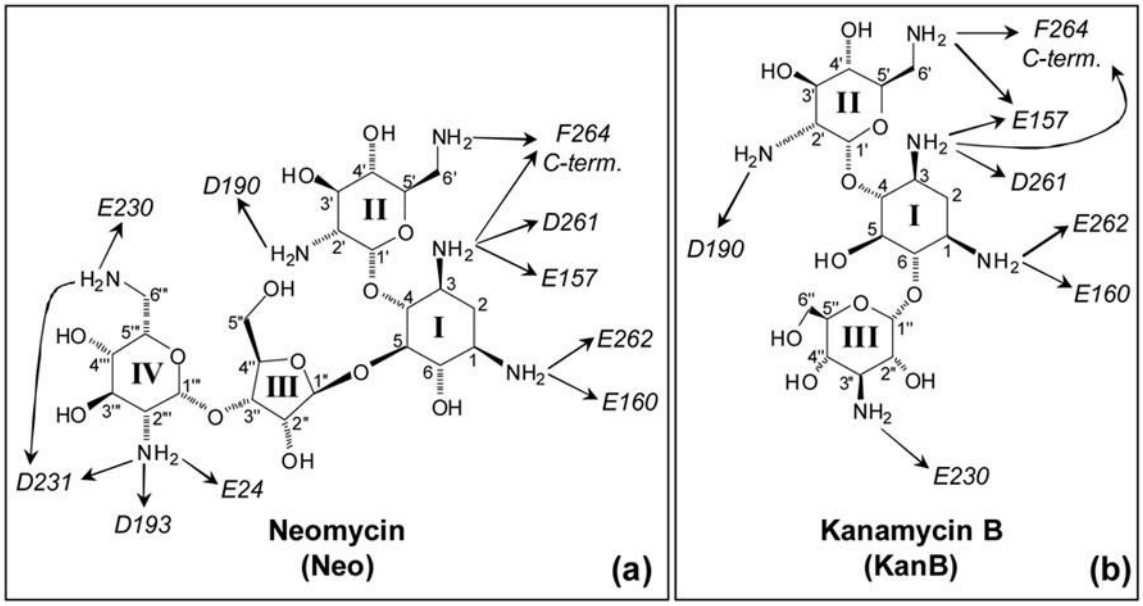

Figure 1.

Structures of Neo (a) and KanB (b), with the atomic and ring numbering systems denoted in Arabic and Roman numerals, respectively. The APH(3′)-IIIa amino acid residues that crystallographic studies[11] indicate form electrostatic contacts with the drug amino groups are indicated.

NIH-PA Author Manuscript
NIH-PA Author Manuscript
NIH-PA Author Manuscript

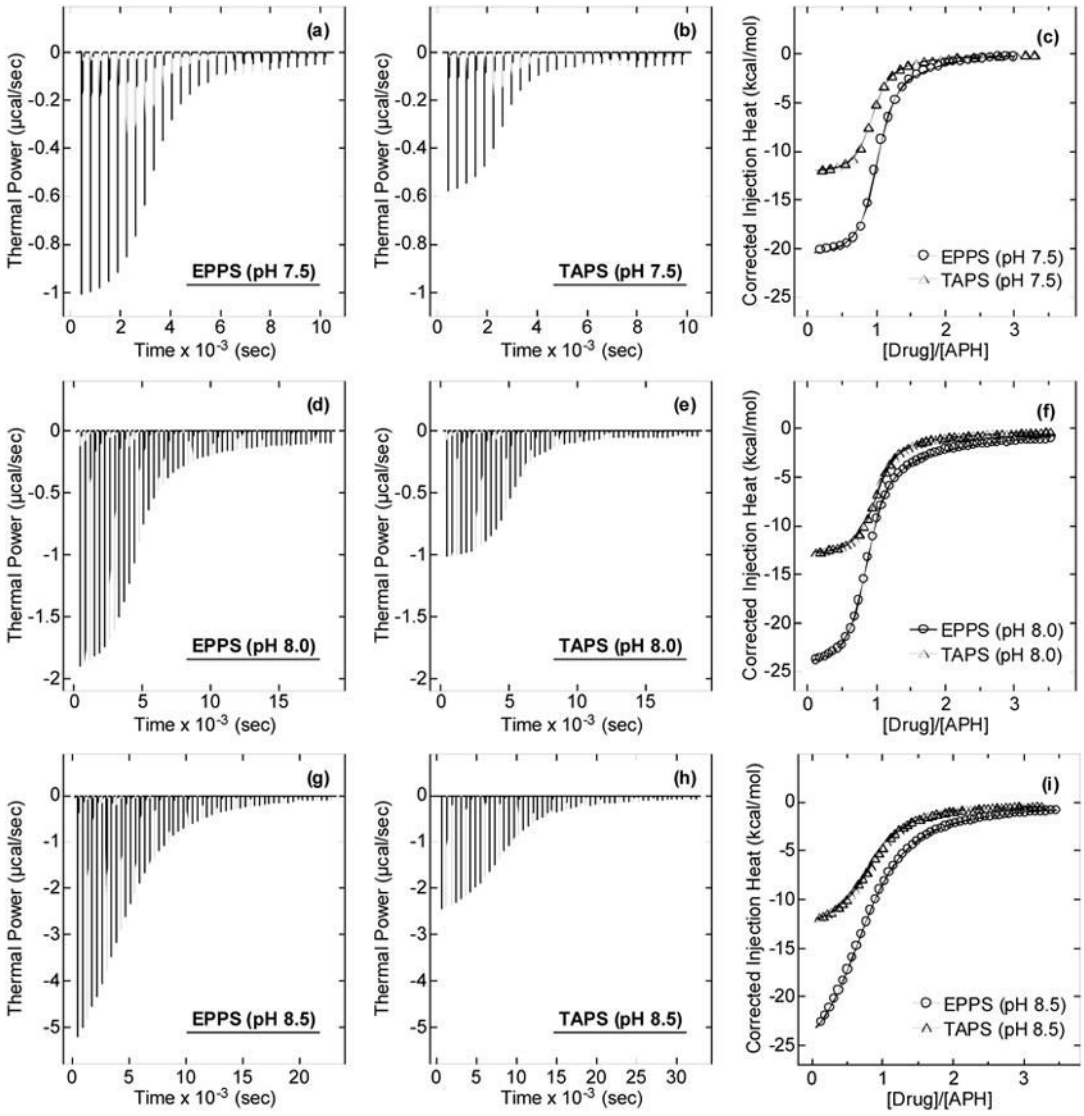

Figure 2.

ITC profiles at 25 °C for the titration of Neo into wt APH(3′)-IIIa at pH 7.5 ((a)–(c)), 8.0 ((d)–(f)), and 8.5 ((g)–(i)) in either EPPS or TAPS buffer. The drug dilution-corrected injection heats shown in panels (c), (f), and (i) were fit with a model for two independent sets of binding sites. Each experimental solution contained 10 mM buffer, 100 mM KCl, 5 mM $MgCl_2$, and 0.01% TWEEN 80.

NIH-PA Author Manuscript

NIH-PA Author Manuscript

NIH-PA Author Manuscript

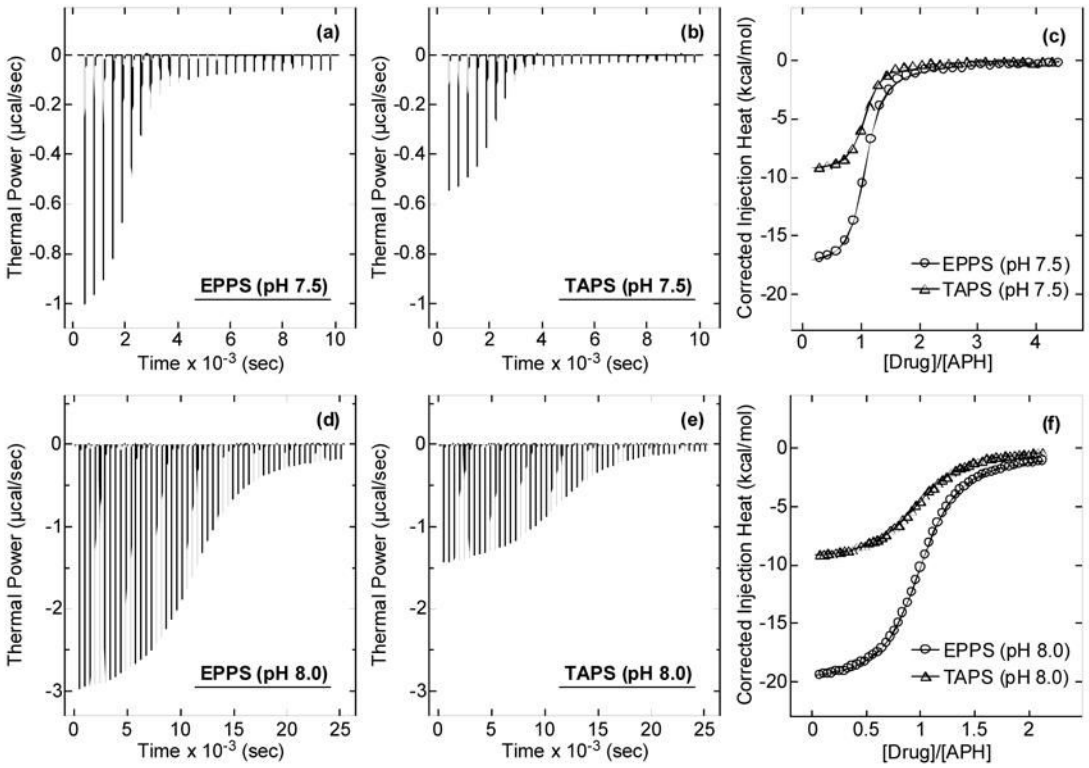

Figure 3.

ITC profiles at 25 °C for the titration of KanB into wt APH(3′)-IIIa at pH 7.5 ((a)–(c)) and 8.0 ((d)–(f)) in either EPPS or TAPS buffer. The drug dilution-corrected injection heats shown in panels (c) and (f) were fit with a model for two independent sets of binding sites. Solution conditions were as described in the legend to Figure 2.

NIH-PA Author Manuscript

NIH-PA Author Manuscript

NIH-PA Author Manuscript

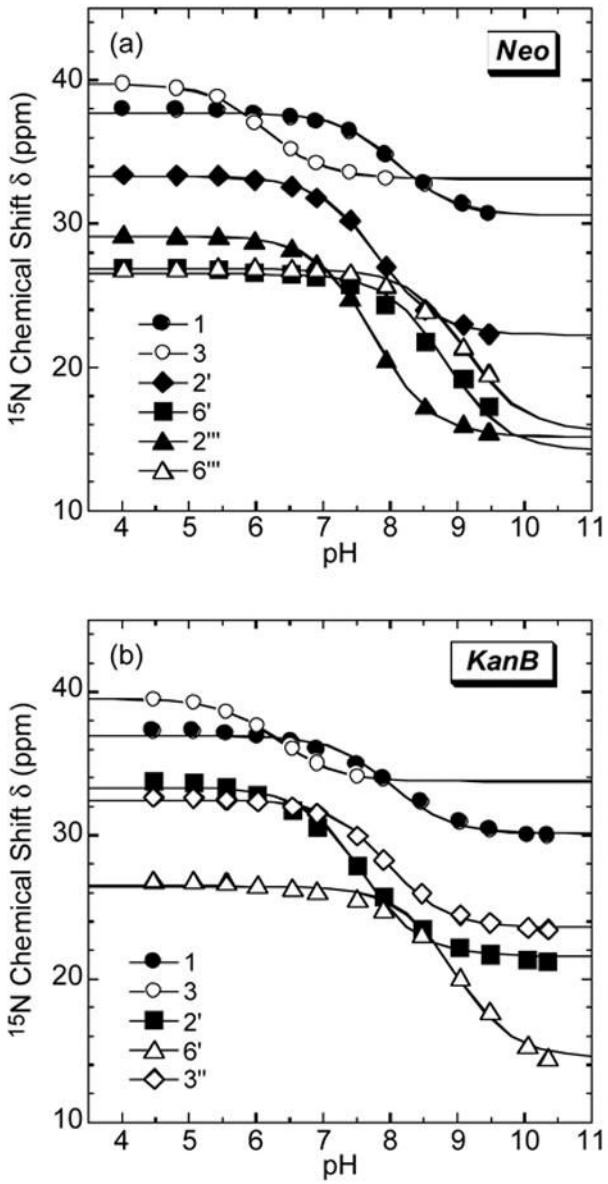

Figure 4.

pH dependence of the ^{15}N chemical shifts (δ) of the free base forms of Neo (a) and KanB (b) at 25 °C. The continuous lines reflect the calculated fits of the experimental data using equation (2).

NIH-PA Author Manuscript

NIH-PA Author Manuscript

NIH-PA Author Manuscript

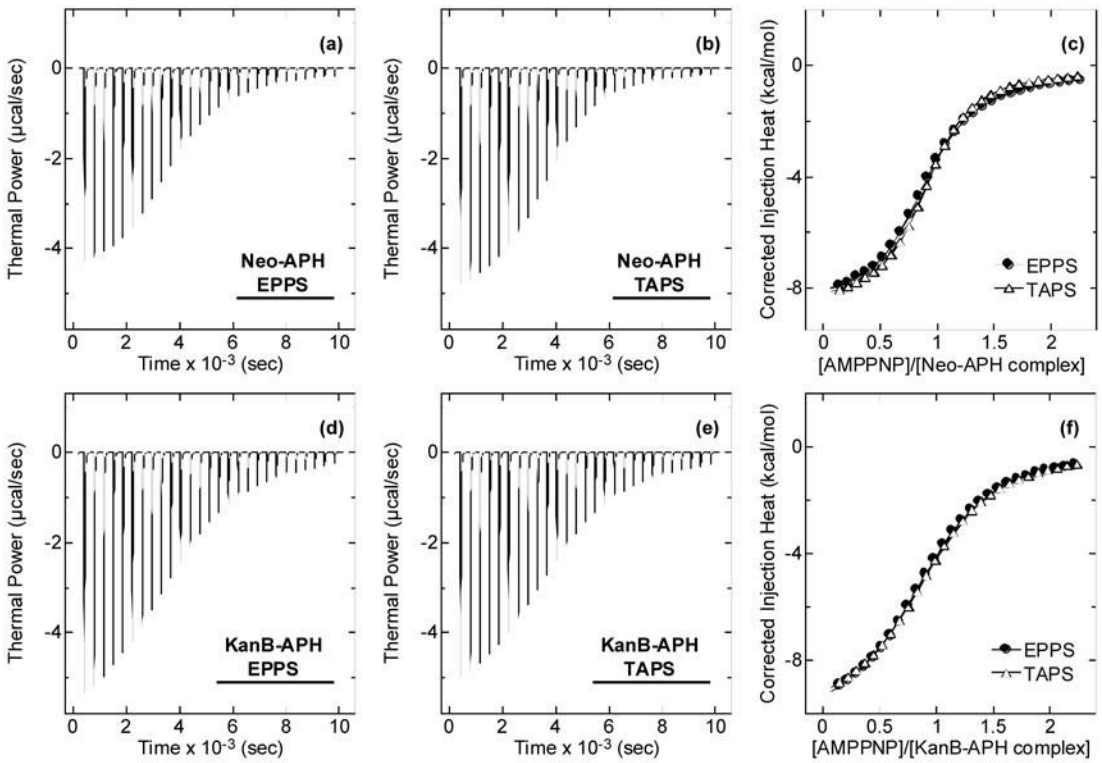

Figure 5.

ITC profiles at pH 8.0 and 25 °C for the titration of AMP-PNP into the Neo-APH(3′)-IIIa ((a)–(c)) and KanB-APH(3′)-IIIa ((d)–(f)) complexes in either EPPS or TAPS buffer. The cofactor dilution-corrected injection heats shown in panels (c) and (f) were fit with a model for one set of binding sites. The solution conditions were as described in the legend to Figure 2.

NIH-PA Author Manuscript
NIH-PA Author Manuscript
NIH-PA Author Manuscript

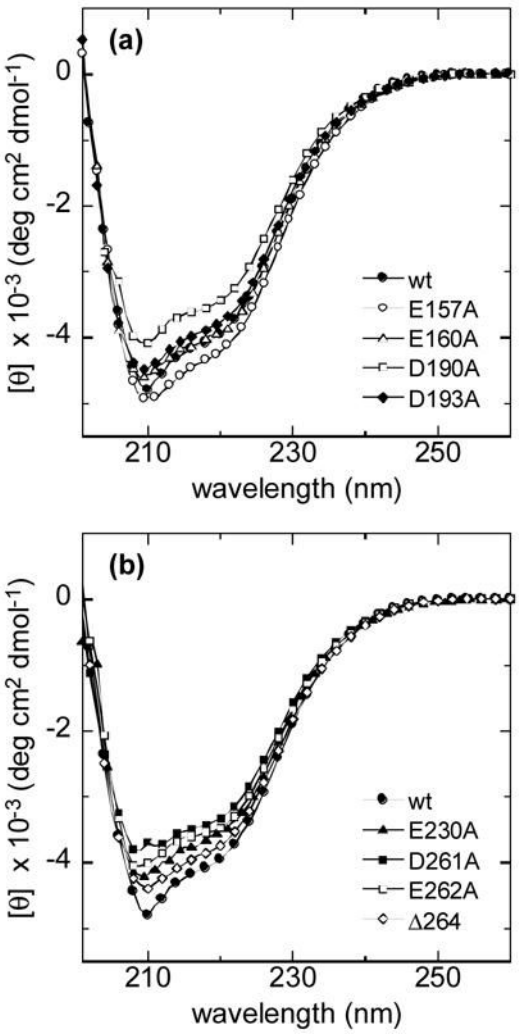

Figure 6.

CD spectra of wt APH(3′)-IIIa and the indicated mutant forms of the enzyme. For purposes of clarity, each panel contains the CD spectra of wt APH(3′)-IIIa and four different mutant forms of the enzyme. The CD spectra were acquired at 25 °C in the presence of 10 mM EPPS (pH 7.5), 100 mM KCl and 5 mM $MgCl_2$. The protein concentration was 10 μM.

NIH-PA Author Manuscript
NIH-PA Author Manuscript
NIH-PA Author Manuscript

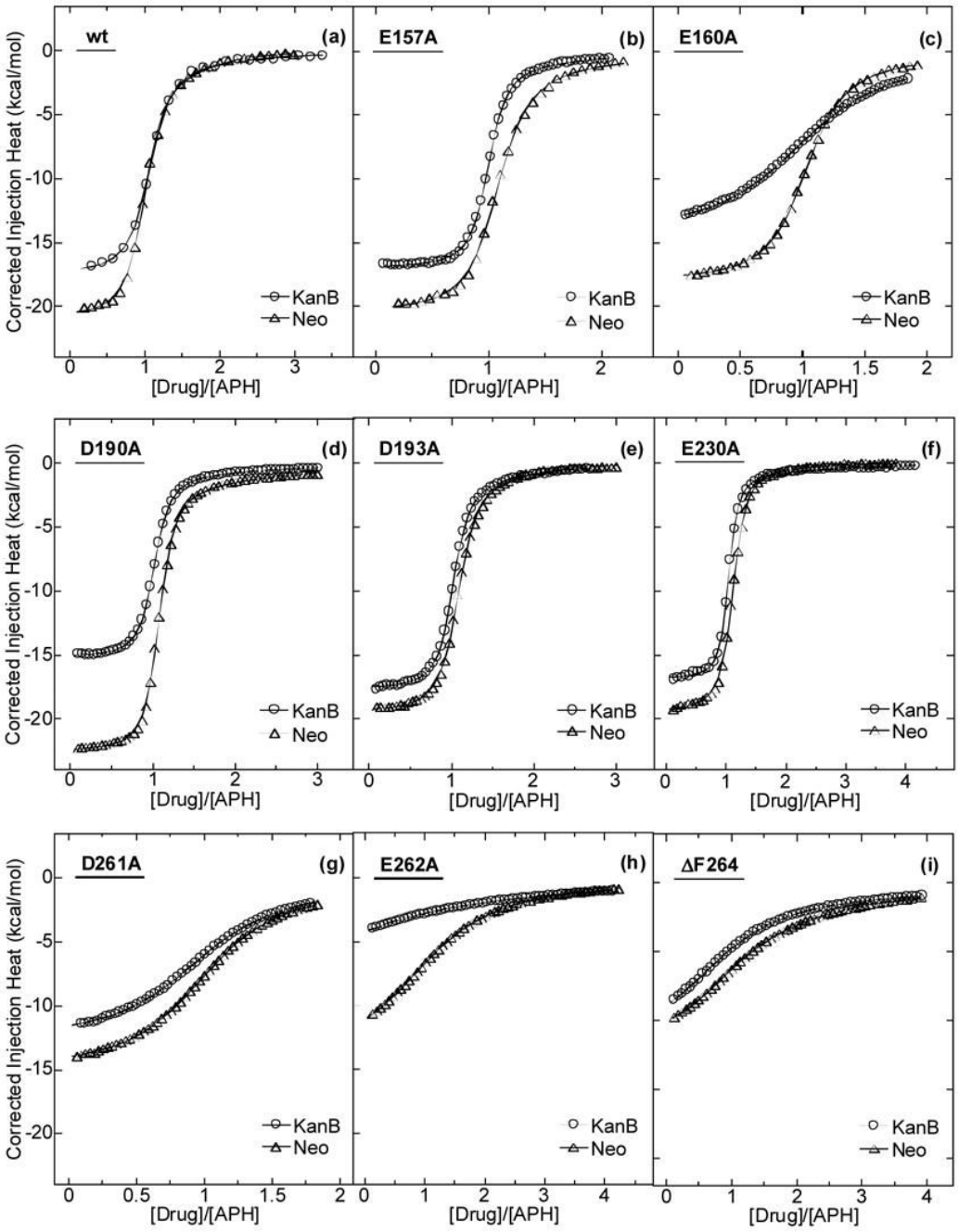

Figure 7.

Drug dilution-corrected ITC profiles (acquired at pH 7.5 and 25 °C) for the binding of Neo (Δ) and KanB (○) to wt APH(3′)-IIIa (a), as well as to the indicated mutant forms of the enzyme ((b) –(i)). The drug dilution-corrected injection heats were fit with a model for two independent sets of binding sites. The solution conditions were 10 mM EPPS, 100 mM KCl, 5 mM $MgCl_2$, and 0.01% TWEEN 80.

NIH-PA Author Manuscript

NIH-PA Author Manuscript

NIH-PA Author Manuscript

Table 1

ITC-derived parameters for the binding of Neo and KanB to APH(3′)-IIIa at 25 °C

PH	Buffer	K_1 (M^{-1})	ΔH_1 (kcal/mol)	N_1	K_2 (M^{-1})	ΔH_2 (kcal/mol)	N_2
			Neo				
7.5	EPPS	$(4.2 \pm 1.5) \times 10^7$	−20.8 ± 0.1	1.0	$(7.1 \pm 2.6) \times 10^5$	−2.0 ± 0.2	1.0
	TAPS	$(3.1 \pm 0.6) \times 10^7$	−12.3 ± 0.1	0.9	$(4.7 \pm 1.1) \times 10^5$	−1.0 ± 0.1	1.0
8.0	EPPS	$(2.6 \pm 0.1) \times 10^6$	−24.5 ± 0.1	0.9	$(3.0 \pm 0.2) \times 10^4$	−8.9 ± 0.1	1.0
	TAPS	$(2.9 \pm 0.1) \times 10^6$	−13.0 ± 0.1	1.0	$(2.5 \pm 0.2) \times 10^4$	−3.6 ± 0.1	1.0
8.5	EPPS	$(1.0 \pm 0.1) \times 10^5$	−27.8 ± 0.1	0.8	$(3.6 \pm 0.3) \times 10^3$	−5.8 ± 0.2	1.0
	TAPS	$(1.7 \pm 0.1) \times 10^5$	−13.1 ± 0.1	0.9	$(1.9 \pm 0.7) \times 10^3$	−4.5 ± 1.1	1.0
			KanB				
7.5	EPPS	$(1.7 \pm 0.2) \times 10^7$	−17.4 ± 0.1	1.0	$(2.1 \pm 0.4) \times 10^5$	−2.4 ± 0.2	1.0
	TAPS	$(1.8 \pm 0.4) \times 10^7$	−9.4 ± 0.1	1.0	$(2.0 \pm 0.8) \times 10^5$	−0.8 ± 0.1	1.0
8.0	EPPS	$(6.2 \pm 1.5) \times 10^5$	−20.0 ± 0.1	1.0	$(5.3 \pm 0.5) \times 10^3$	−4.8 ± 0.3	1.0
	TAPS	$(3.7 \pm 0.3) \times 10^5$	−9.6 ± 0.1	1.0	$(4.6 \pm 1.6) \times 10^3$	−0.9 ± 0.1	1.0

The ITC profiles shown in Figures 2 and 3 were fit with a model for two independent sets of binding sites using K_1, ΔH_1, K_2, and ΔH_2 as free-floating parameters. The values of N_1 and N_2 were fixed during the fitting routines and manually varied to yield the best fit (as reflected by minimization of χ^2). The indicated uncertainties in K_1, ΔH_1, K_2, and ΔH_2 reflect the standard deviation of the experimental data from the fitted curves.

NIH-PA Author Manuscript

NIH-PA Author Manuscript

NIH-PA Author Manuscript

Table 2

pH-Dependence of the number of protons linked to the binding of Neo and KanB to wt APH(3′)-IIIa at 25 °C

pH	ΔH_{corr} (± 0.3) (kcal/mol)	Δn (± 0.04)
	Neo	
7.5	−30.0	1.78
8.0	−37.0	2.41
8.5	−43.7	3.08
	KanB	
7.5	−26.0	1.68
8.0	−31.2	2.18

Values of Δn and ΔH_{corr} were calculated by simultaneous solution of equations 1(a) and (b). In application of these equations, the ΔH_{ion} values for EPPS and TAPS (+5.15 and +9.92 kcal/mol respectively) were taken from Fukada and Takahashi,[13] while the values of ΔH_{obs} corresponded to the values of ΔH_1 listed in Table 1.

NIH-PA Author Manuscript

NIH-PA Author Manuscript

NIH-PA Author Manuscript

Table 3

^{15}N NMR-derived pK_a values for the amino groups of the free base forms of Neo and KanB at 25 °C

Amino Group	pK_a	
	Neo	KanB
1	8.10 ± 0.05	8.00 ± 0.07
3	6.16 ± 0.03	6.34 ± 0.03
2′	7.80 ± 0.02	7.57 ± 0.05
6′	8.83 ± 0.08	8.96 ± 0.06
3″	n.a.	7.95 ± 0.03
2‴	7.75 ± 0.02	n.a.
6‴	9.13 ± 0.05	n.a.

pK_a values of the amino groups were derived from fits of the pH-dependent ^{15}N chemical shift data shown in Figure 4 using equation (2). The indicated uncertainties reflect the standard deviations of the experimental data from the fitted curves. n.a. denotes not applicable.

NIH-PA Author Manuscript

NIH-PA Author Manuscript

NIH-PA Author Manuscript

Table 4

Changes in the total energies of the Neo-APH(3′)-IIIa and KanB-APH(3′)-IIIa complexes associated with the systematic conversion of each drug amino group from the NH_3^+ to the NH_2 state

NH_2 Group	ΔE_{tot} (kcal/mol)
KanB	
1	+332
3	+325
2′	+271
6′	+169
3″	+88
Neo	
3	+447
2‴	+420
2′	+376
6‴	+330
6′	+316
1	+299

Changes in total energy (ΔE_{tot}) were calculated by subtracting E_{tot} of the complex formed between APH(3′)-IIIa and the fully-protonated form of the drug from the corresponding E_{tot} of the complex formed between APH(3′)-IIIa and the drug containing the indicated amino group in its deprotonated NH_2 form.

NIH-PA Author Manuscript

NIH-PA Author Manuscript

NIH-PA Author Manuscript

Table 5

ITC-derived parameters for the binding of AMP-PNP to the KanB-APH(3′)-IIIa and Neo-APH(3′)-IIIa complexes at pH 8.0 and 25 °C

Complex	Buffer	*N*	K_a (M^{-1})	ΔH_{obs} (kcal/mol)
KanB-APH(3′)-IIIa	EPPS	1.0 ± 0.1	$(4.7 \pm 0.1) \times 10^4$	−10.5 ± 0.1
	TAPS	1.0 ± 0.1	$(5.1 \pm 0.1) \times 10^4$	−10.3 ± 0.1
Neo-APH(3′)-IIIa	EPPS	0.9 ± 0.1	$(7.2 \pm 0.4) \times 10^4$	−9.0 ± 0.1
	TAPS	0.9 ± 0.1	$(1.1 \pm 0.1) \times 10^5$	−8.7 ± 0.1

Values of *N*, K_a, and ΔH_{obs} were derived from the fits of the ITC profiles shown in Figure 5 with a model for one set of binding sites, with the indicated uncertainties reflecting the standard deviations of the experimental data from the fitted curves.

NIH-PA Author Manuscript

NIH-PA Author Manuscript

NIH-PA Author Manuscript

Table 6

Impact of APH(3′)-IIIa mutations on resistance, enzyme-drug binding affinity, and catalysis

APH(3′)-IIIa	MIC (μM)[a]	K_a (M^{-1})[b]	K_m (μM)[c]	k_{cat} (s^{-1})[c]
		Neo		
none	6	n.a.	n.a.	n.a.
wt	1600	$(4.2 \pm 1.5) \times 10^7$	18.2 ± 1.6	1.7 ± 0.1
E157A	800	$(7.6 \pm 0.2) \times 10^6$	14.7 ± 1.7	1.3 ± 0.1
E160A	1600	$(1.4 \pm 0.1) \times 10^6$	25.2 ± 5.1	2.4 ± 0.2
D190A	6	$(1.9 \pm 0.2) \times 10^6$	n.d.	n.d.
D193A	200	$(1.9 \pm 0.4) \times 10^7$	5.9 ± 1.0	0.7 ± 0.1
E230A	1600	$(9.1 \pm 3.4) \times 10^6$	10.0 ± 1.0	1.3 ± 0.1
D261A	12	$(1.3 \pm 0.3) \times 10^5$	3.3 ± 1.5	0.02 ± 0.01
E262A	6	$(2.1 \pm 0.1) \times 10^4$	21.2 ± 5.1	1.9 ± 0.1
ΔF264	12	$(1.4 \pm 0.1) \times 10^4$	10.7 ± 1.8	0.9 ± 0.1
		KanB		
none	6	n.a.	n.a.	n.a.
wt	1600	$(1.7 \pm 0.2) \times 10^7$	19.3 ± 6.8	1.9 ± 0.2
E157A	800	$(2.2 \pm 0.9) \times 10^7$	44.1 ± 5.7	2.5 ± 0.1
E160A	400	$(2.1 \pm 0.1) \times 10^5$	42.9 ± 7.2	2.7 ± 0.2
D190A	6	$(1.8 \pm 0.1) \times 10^6$	n.d.	n.d.
D193A	1600	$(1.3 \pm 0.1) \times 10^7$	38.7 ± 9.1	2.7 ± 0.2
E230A	1600	$(1.1 \pm 0.1) \times 10^7$	39.8 ± 4.5	2.1 ± 0.1
D261A	12	$(1.4 \pm 0.1) \times 10^5$	9.1 ± 1.0	0.2 ± 0.01
E262A	6	$(2.2 \pm 0.6) \times 10^3$	36.4 ± 4.6	1.2 ± 0.1
ΔF264	12	$(6.3 \pm 0.2) \times 10^3$	16.4 ± 3.0	0.9 ± 0.1

[a] Antibacterial activities were assayed in at least two independent experiments. For each drug, the MIC (minimal inhibitory concentration) value obtained was identical in each of the experiments.

[b] Values of K_a were derived from fits of the ITC profiles shown in Figure 7. The indicated uncertainties reflect the standard deviations of the experimental data from the fitted curves. n.a. denotes not applicable.

[c] Values of K_m and k_{cat} were derived from the fits of v versus [S] plots as described in the Materials and Methods, with the indicated uncertainties reflecting the standard deviations of the experimental data from the fitted curves. n.d. denotes not detectable.